Journal of Ceramic Processing Research. Vol. 13, No. 6, pp. 825~829 (2012)

J O U R N A L O F
Ceramic Processing Research

Fabrication and characterization of upconversion photoluminescence $CaMoO_4$:Er^{3+}/Yb^{3+} particles by a cyclic microwave-assisted metathetic method

Chang Sung Lim*

Department of Advanced Materials Science & Engineering, Hanseo University, Seosan 356-706, Korea

Er^{3+}/Yb^{3+} co-doped $CaMoO_4$ ($CaMoO_4$:Er^{3+}/Yb^{3+}) particles were successfully synthesized by a cyclic microwave-assisted metathetic (MAM) method, followed by further heat-treatment. Well-crystallized $CaMoO_4$:Er^{3+}/Yb^{3+} particles were formed after heat-treatment at 600 °C for 3 h, and showed a fine and homogeneous morphology with sizes of 0.2-1 μm. With excitation at 980 nm, $CaMoO_4$:Er^{3+}/Yb^{3+}# exhibited a strong 525-nm emission band and a weak 550-nm emission band in the green region, and a weak 655-nm emission band in the red region. The upconversion (UC) intensity of $CaMoO_4$:Er^{3+}/Yb^{3+}# particles was much higher than those of the $CaMoO_4$:Er^{3+} and $CaMoO_4$:Er^{3+}/Yb^{3+} particles. The Raman spectra of $CaMoO_4$:Er^{3+}, $CaMoO_4$:Er^{3+}/Yb^{3+}, $CaMoO_4$:Er^{3+}/Yb^{3+}# and $CaMoO_4$:Er^{3+}/Yb^{3+}## particles indicated the detection of additional strong peaks at higher frequencies (618, 575, 492, 420 and 373 cm^{-1}) and at lower frequencies (290 and 234 cm^{-1}).

Key words: Upconversion photoluminescence, $CaMoO_4$:Er^{3+}/Yb^{3+} particles, Cyclic microwave, Metathetic method, Raman spectroscopy.

Introduction

Upconversion (UC) photoluminescence particles can convert near infrared radiation of low energy into visible radiation of high energy. Recently, these UC photoluminescence particles have evolved in their applications, showing great potential for imaging and biodetection assays in both in vitro and in vivo with their high penetration depth into tissues, sharp emission bands, and high resistance to photobleaching, which overcome the current limitations in traditional photoluminescence materials [1-3]. Particles of rare earth-doped UC $CaMoO_4$, which is at type of metallic molybdate compound with a schleelite-type structure of lattice parameters a = b = 5.212 Å and c = 11.438 Å [4-6], are relatively stable in air and have stable physical and chemical properties, low excitation threshold energy, and low-cost production. Energy transfer plays a crucial role in luminescent materials because it varies the luminescent intensity depending on the co-doped ion. Rare earth ions, such as Yb^{3+} and Er^{3+} ions, act as efficient sensitizers or activators that transfer energy in several host lattices. The Yb^{3+} ion as a sensitizer can be excited effectively by the energy of the incident light source, and this excitation transfers this energy to the activator, which emits radiation. The co-doped Yb^{3+} ion and Er^{3+} ion can remarkably enhance the UC efficiency from infrared to visible light due to the efficient energy transfer from Yb^{3+} to Er^{3+} [7-9].

*Corresponding author:
Tel : +82-41-660-1445
Fax: +82-41-660-1445
E-mail: cslim@hanseo.ac.kr

Recently, several processes have been developed to increase the applications of rare-earth-doped metal molybdates prepared using a range of processes, including solid-state reactions [10-14], co-precipitation [15], the sol-gel method [16], the hydrothermal method [17-19], the Pechini method [20], the solvothermal route [21] and the microwave-assisted hydrothermal method [22]. For practical application of UC photoluminescence in such products as lasers, three-dimensional displays, light emitting devices, and biological detectors, features such as homogeneous UC particle size distribution and morphology need to be well defined. Compared with the usual methods, microwave synthesis has the advantages of a very short reaction time, small-size particles and narrow particle size distribution, and high purity for preparing polycrystalline samples. Microwave energy is delivered directly to the material by molecular interactions under an electric field. Therefore, it is possible to rapidly and uniformly heat thick materials. Cyclic microwave-assisted metathetic (MAM) synthesis of materials is a simple and cost-effective method that provides a high yield with easy scale up, and is emerging as a viable alternative approach for the synthesis of high-quality novel inorganic materials in short time periods [6, 23].

In this study, Er^{3+}/Yb^{3+} co-doped $CaMoO_4$ ($CaMoO_4$:Er^{3+}/Yb^{3+}) particles were synthesized by the cyclic MAM route, followed by heat-treatment. The synthesized $CaMoO_4$:Er^{3+}/Yb^{3+} particles were characterized by X-ray diffraction (XRD), scanning electron microscopy (SEM) and energy-dispersive X-ray spectroscopy (EDS). Optical properties were examined by using photoluminescence (PL) emission data and Raman spectroscopy.

Experimental

Appropriate stoichiometric amounts of $CaCl_2$, $ErCl_3 \cdot 6H_2O$, $YbCl_3 \cdot 6H_2O$, $Na_2MoO_4 \cdot 2H_2O$ and ethylene glycol of analytic reagent grade were used to prepare the $CaMoO_4$, $CaMoO_4$:Er^{3+}, $CaMoO_4$:Er^{3+}/Yb^{3+}, $CaMoO_4$:Er^{3+}/Yb^{3+}# and $CaMoO_4$:Er^{3+}/Yb^{3+}## compounds. To prepare $CaMoO_4$, 1 mol% $CaCl_2$ and 1 mol% $Na_2MoO_4 \cdot 2H_2O$ were dissolved in 30 ml ethylene glycol. To prepare $CaMoO_4$:Er^{3+}, 0.95 mol% $CaCl_2$ with 0.05 mol% $ErCl_3 \cdot 6H_2O$ and 1 mol% $Na_2MoO_4 \cdot 2H_2O$ were dissolved in 30 ml ethylene glycol. To prepare $CaMoO_4$:Er^{3+}/Yb^{3+}, 0.9 mol% $CaCl_2$ with 0.05 mol% $ErCl_3 \cdot 6H_2O$ and 0.05 mol% $YbCl_3 \cdot 6H_2O$ and 1 mol% $Na_2MoO_4 \cdot 2H_2O$ were dissolved in 30 ml ethylene glycol. To prepare $CaMoO_4$:Er^{3+}/Yb^{3+}#, 0.8 mol% $CaCl_2$ with 0.02 mol% $ErCl_3 \cdot 6H_2O$ and 0.18 mol% $YbCl_3 \cdot 6H_2O$ and 1 mol% $Na_2MoO_4 \cdot 2H_2O$ were dissolved in 30 ml ethylene glycol. To prepare $CaMoO_4$:Er^{3+}/Yb^{3+}##, 0.78 mol% $CaCl_2$ with 0.02 mol% $ErCl_3 \cdot 6H_2O$ and 0.2 mol% $YbCl_3 \cdot 6H_2O$ and 1 mol% $Na_2MoO_4 \cdot 2H_2O$ were dissolved in 30 ml ethylene glycol.

The solutions were mixed and adjusted to pH 9.5 using NaOH. The aqueous solutions were stirred at room temperature. The mixtures were transferred into 120 ml Teflon vessels, respectively. Each Teflon vessel was placed into a microwave oven operating at a frequency of 2.45 GHz with a maximum output power of 1250 W for 23 minutes. The working cycle of the MAM reaction was controlled very precisely between 30 seconds on and 30 seconds off for 8 minutes, followed by a further treatment of 30 seconds on and 60 seconds off for 15 minutes. The ethylene glycol was evaporated slowly at its boiling point. Ethylene glycol, a polar solvent at its boiling point of 197 °C, is a good candidate for the microwave process. When ethylene glycol is used as the solvent, reactions proceed at the boiling point temperature. The microwave radiation is supplied to ethylene glycol, and the components dissolving in the ethylene glycol couple with each other under the radiation. When a large amount of microwave radiation is supplied to the ethylene glycol, the charged particles vibrate interdependently within the electric field. The resulting samples were treated with ultrasonic radiation and washed many times with hot distilled water. The white precipitates were collected and dried at 100 °C in a drying oven. The final products were heat-treated at 600 °C for 3 h.

The phase of the particles after the cyclic MAM reaction and heat-treatment was identified using XRD (D/MAX 2200, Rigaku, Japan). The microstructures and surface morphologies of the $CaMoO_4$, $CaMoO_4$:Er^{3+}, $CaMoO_4$:Er^{3+}/Yb^{3+}, $CaMoO_4$:Er^{3+}/Yb^{3+}# and $CaMoO_4$:Er^{3+}/Yb^{3+}## particles were observed by using SEM/EDS (JSM-5600, JEOL, Japan). Their PL spectra were recorded using a spectrophotometer (Perkin Elmer LS55, UK) at room temperature. Raman spectroscopy measurements were performed using a LabRam HR (Jobin-Yvon, France). The 514.5 nm line of an Ar-ion laser was used as the excitation source, and the power on the samples was kept at 0.5 mW.

Results and Discussion

Fig. 1 shows the XRD patterns of the synthesized (a) $CaMoO_4$:Er^{3+}, (b) $CaMoO_4$:Er^{3+}/Yb^{3+} and (c) $CaMoO_4$:Er^{3+}/Yb^{3+}# particles. All of the XRD peaks could be assigned to the tetragonal-phase $CaMoO_4$ with a scheelite-type structure, which was in good agreement with the crystallographic data of $CaMoO_4$ (JCPDS 85-0585). This finding means that the tetragonal-phase $CaMoO_4$ can be prepared using the cyclic MAM route. Post heat-treatment plays an important role in a well-defined crystallized morphology. To achieve a well-defined crystalline morphology, the $CaMoO_4$ phases need to be heat treated at 600 °C for 3 h. The $CaMoO_4$ formed by the Pechini method had a scheelite-type crystal structure with lattice parameters of a = b = 5.212 Å and c = 11.438 Å. This finding suggests that the cyclic MAM route is suitable for growing $CaMoO_4$ crystallites and for developing the strongest intensity peaks of the (101), (112) and (312) planes, which are the major peaks of $CaMoO_4$ [4-6]. The widths of the peaks increase slightly according to the amount of doping with Yb^{3+} in the cases of (b) $CaMoO_4$:Er^{3+}/Yb^{3+} and (c) $CaMoO_4$:Er^{3+}/Yb^{3+}#. It is assumed that the doping amount of Er^{3+}/Yb^{3+} has a great effect on the crystalline cell volume of the $CaMoO_4$, because of the different ionic sizes and valence states.

Fig. 2 shows SEM images of the (a) $CaMoO_4$, (b) $CaMoO_4$:Er^{3+}, (c) $CaMoO_4$:Er^{3+}/Yb^{3+} and (d) $CaMoO_4$:Er^{3+}/Yb^{3+}# particles after the cyclic MAM route followed by further heat-treatment at 600 °C for 3 h. The as-synthesized samples are well crystallized with a fine and homogeneous morphology with particles of different sizes of 1-4 μm for the (a) $CaMoO_4$ and 0.2-1 μm for the (b) $CaMoO_4$:Er^{3+}, (c) $CaMoO_4$:Er^{3+}/Yb^{3+}

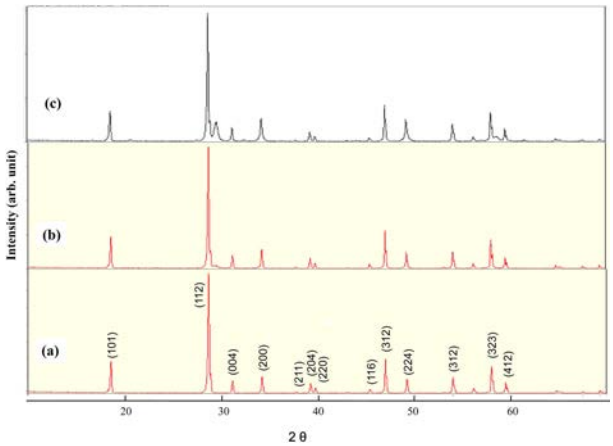

Fig. 1. X-ray diffraction patterns of the synthesized (a) $CaMoO_4$:Er^{3+}, (b) $CaMoO_4$:Er^{3+}/Yb^{3+} and (c) $CaMoO_4$:Er^{3+}/Yb^{3+}# particles.

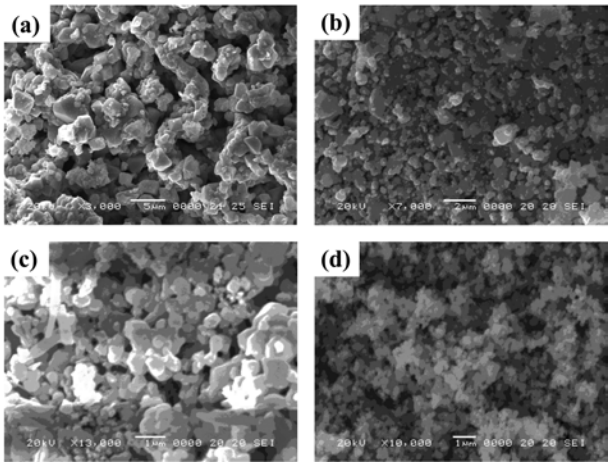

Fig. 2. Scanning electron microscopy images of the synthesized (a) $CaMoO_4$, (b) $CaMoO_4:Er^{3+}$, (c) $CaMoO_4:Er^{3+}/Yb^{3+}$ and (d) $CaMoO_4:Er^{3+}/Yb^{3+}$# particles.

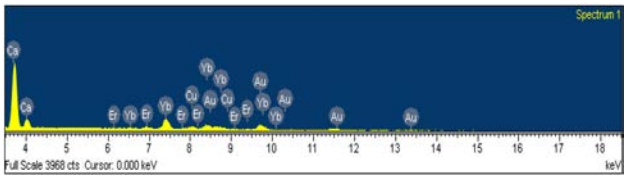

Fig. 3. Energy-dispersive X-ray spectroscopy patterns of the synthesized $CaMoO_4:Er^{3+}/Yb^{3+}$# particles.

and (d) $CaMoO_4:Er^{3+}/Yb^{3+}$#. The samples of (a) $CaMoO_4$, (b) $CaMoO_4:Er^{3+}$ and (c) $CaMoO_4:Er^{3+}/Yb^{3+}$ show a well-crystallized morphology, while the sample of (d) $CaMoO_4:Er^{3+}/Yb^{3+}$# shows a scattered morphology with an obvious discrepancy in crystallization and particle size. This discrepancy means that the amounts of doping of the 0.05 mol% Er^{3+} for $CaMoO_4:Er^{3+}$ and 0.05 mol% Er^{3+} and 0.05 mol% Yb^{3+} for $CaMoO_4:Er^{3+}/Yb^{3+}$ have little effect on the morphological features. However, $CaMoO_4:Er^{3+}/Yb^{3+}$# (d) compared to $CaMoO_4:Er^{3+}$ (b) and $CaMoO_4:Er^{3+}/Yb^{3+}$ (c) has a somewhat different shape. The amounts of doping of 0.02 mol% Er^{3+} and 0.18 mol% Yb^{3+} for $CaMoO_4:Er^{3+}/Yb^{3+}$# have a great effect on the morphological features. Fig. 3 shows the EDS pattern of the synthesized $CaMoO_4:Er^{3+}/Yb^{3+}$# particles. The EDS pattern shows that the $CaMoO_4:Er^{3+}/Yb^{3+}$# particles are composed of Ca, Mo, O, Er and Yb. MAM reactions, such as $CaCl_2 + Na_2MoO_4 \rightarrow CaMoO_4 + 2NaCl$, involve the exchange of atomic/ionic species, in which the driving force is the exothermic reaction accompanying the formation of NaCl [24, 25]. MAM reactions occur so rapidly that the exothermic reaction is essentially used to heat up the solid products. The cyclic MAM reactions provide a convenient route for the synthesis of $CaMoO_4$, $CaMoO_4:Er^{3+}$, $CaMoO_4:Er^{3+}/Yb^{3+}$, $CaMoO_4:Er^{3+}/Yb^{3+}$# and $CaMoO_4:Er^{3+}/Yb^{3+}$## particles. The cyclic MAM route of metal molybdates [26, 27] provides the exothermic energy to synthesize the bulk of the material uniformly, so that fine particles with a controlled

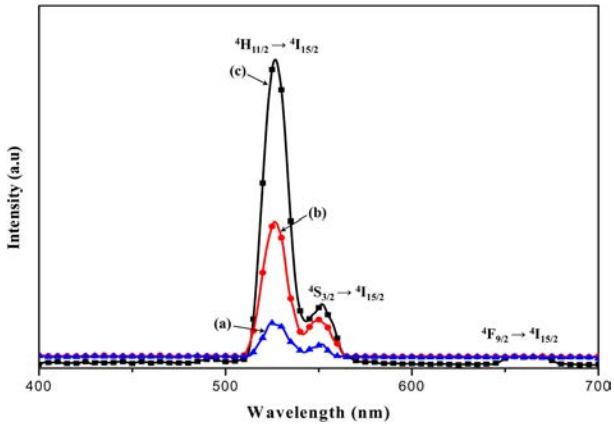

Fig. 4. UC photoluminescence emission spectra of the synthesized (a) $CaMoO_4:Er^{3+}$ (CMO:Er), (b) $CaMoO_4:Er^{3+}/Yb^{3+}$ (CMO:Er/Yb) and (c) $CaMoO_4:Er^{3+}/Yb^{3+}$# (CMO:Er/Yb#) particles excited at 980 nm at room temperature.

morphology can be fabricated in an environmentally-friendly manner without the generation of solvent waste. $CaMoO_4:Er^{3+}$, $CaMoO_4:Er^{3+}/Yb^{3+}$, $CaMoO_4:Er^{3+}/Yb^{3+}$# and $CaMoO_4:Er^{3+}/Yb^{3+}$## particles, as well as $CaMoO_4$ particles, were heated rapidly and uniformly by the cyclic MAM route. Therefore, this method is a simple and cost-effective method that can provide high yields with easy scale up, thus emerging as a viable alternative in the rapid synthesis of UC particles.

Fig. 4 shows the UC photoluminescence emission spectra of (a) $CaMoO_4:Er^{3+}$ (CMO:Er), (b) $CaMoO_4:Er^{3+}/Yb^{3+}$ (CMO:Er/Yb) and (c) $CaMoO_4:Er^{3+}/Yb^{3+}$# (CMO:Er/Yb#) particles excited at 980 nm. The strong emission band of 525 nm and the weak emission band of 550 nm in the green region are assigned to the transitions $^2H_{11/2} \rightarrow {}^4I_{15/2}$ and $^4S_{3/2} \rightarrow {}^4I_{15/2}$ of Er^{3+} ions, respectively, while the weak emission band in the red region of 655 nm corresponds to the transition of $^4F_{9/2} \rightarrow {}^4I_{15/2}$. The UC intensity of $CaMoO_4:Er^{3+}/Yb^{3+}$# particles was much higher than those of the $CaMoO_4:Er^{3+}$ and $CaMoO_4:Er^{3+}/Yb^{3+}$ particles. The amounts of doping by Er^{3+}/Yb^{3+} had a great effect on both the morphological features and UC fluorescence intensity. The Yb^{3+} ion as a sensitizer can be effectively excited by the energy of the incident light source, which transfers this energy to the activator, where radiation can be emitted. The Er^{3+} ion as an activator is the luminescence center in UC particles, and the sensitizer enhances the UC luminescence efficiency. The UC intensity of (c) CMO:Er/Yb# is much higher than those of (a) CMO:Er, (b) CMO:Er/Yb. The UC process is a proven successful method for generating visible light from near infrared (NIR) radiation. UC is a nonlinear optical process in which excitation of the lower electronic levels with a low-energy radiation (NIR light) results in higher energy emission (visible or ultraviolet light) at higher electronic levels; thus it is ascribed as an anti-Stockes mechanism. This process requires the absorption of two or more photons to

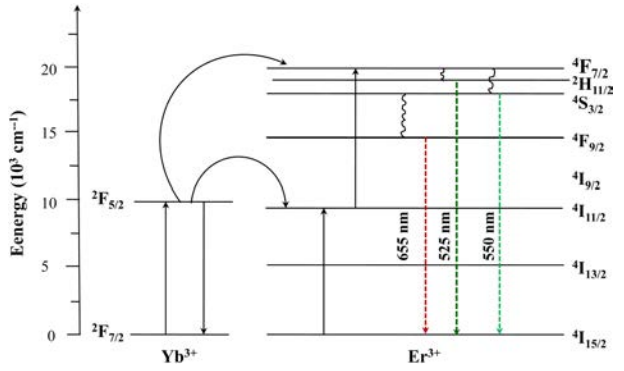

Fig. 5. Schematic energy level diagrams of Er^{3+} ions (activator) and Yb^{3+} ions (sensitizer) in the as-prepared $CaMoO_4:Er^{3+}/Yb^{3+}$ samples and the UC mechanisms accounting for the green and red emissions at 980-nm laser excitation.

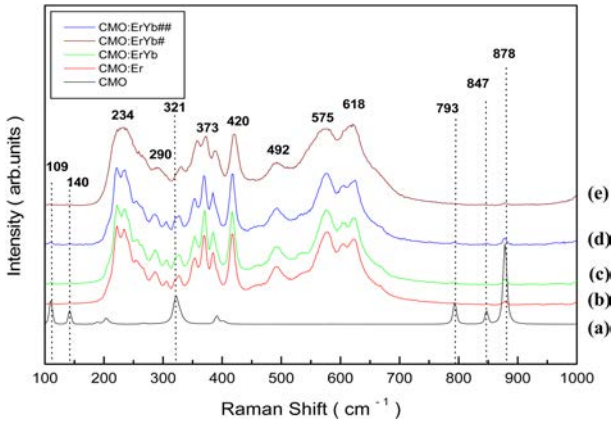

Fig. 6. Raman spectra of the synthesized (a) $CaMoO_4$ (CMO), (b) $CaMoO_4:Er^{3+}$ (CMO:Er), (c) $CaMoO_4:Er^{3+}/Yb^{3+}$ (CMO:Er/Yb), (d) $CaMoO_4:Er^{3+}/Yb^{3+}$# (CMO:Er/Yb#) and (e) $CaMoO_4:Er^{3+}/Yb^{3+}$## (SMO:Er/Yb##) particles excited by the 514.5-nm line of an Ar-ion laser at 0.5 mW on the samples.

produce sufficient energy for UC emission. The different classes of UC processing mechanisms can lead to absorption of two or more photons: excited-state absorption (ESA), energy transfer upconversion (ETU) and photon avalanche (PA) [1-3]. A typical ETU process involves the energy transfer between the two ions, the sensitizer and the activator. The ETU process involves a sequential absorption of two photons that transfers energy from an excited ion (sensitizer) to another neighboring ion (activator), and is independent of the excitation power, so it can be quite efficient under optimized conditions with high dopant ion concentrations.

Fig. 5 shows the schematic energy level diagrams of Er^{3+} ions (activator) and Yb^{3+} ions (sensitizer) in the as-prepared $CaMoO_4:Er^{3+}/Yb^{3+}$ samples and the UC mechanisms accounting for the green and red emissions at 980 nm laser excitation. In the complex Er^{3+}/Yb^{3+} co-doped $CaMoO_4$ system, an initial energy transfer from an Yb^{3+} ion in the $^2F_{5/2}$ state to an Er^{3+} ion populates the $^4I_{11/2}$ level. A second 980 nm photon or the energy transfer from an Yb^{3+} ion can then populate the $^4F_{7/2}$ level of the Er^{3+} ion. The Er^{3+} ion can then relax non-radiatively to the $^2H_{11/2}$ and $^4S_{3/2}$ levels, and green $^2H_{11/2} \rightarrow {}^4I_{15/2}$ and $^4S_{3/2} \rightarrow {}^4I_{15/2}$ emissions occur. Alternatively, the ion can further relax and populate the $^4F_{9/2}$ level, leading to the red $^4F_{9/2} \rightarrow {}^4I_{15/2}$ emission. The $^4F_{9/2}$ level may also be populated from the $^4I_{13/2}$ level of the Er^{3+} ion by absorption of a 980 nm photon, or by energy transfer from an Yb^{3+} ion, with the $^4I_{13/2}$ state being initially populated via the non-radiative $^4I_{11/2} \rightarrow {}^4I_{13/2}$ relaxation [7-9]. The strong 525-nm emission band and the weak 550-nm emission band in the green region are assigned to the $^2H_{11/2} \rightarrow {}^4I_{15/2}$ and $^4S_{3/2} \rightarrow {}^4I_{15/2}$ transitions of Er^{3+} ions, respectively, while the weak 655-nm emission band in the red region is assigned to the $^4F_{9/2} \rightarrow {}^4I_{15/2}$ transition.

Fig. 6 shows the Raman spectra of the (a) $CaMoO_4$ (CMO), (b) $CaMoO_4:Er^{3+}$ (CMO:Er), (c) $CaMoO_4:Er^{3+}/Yb^{3+}$ (CMO:Er/Yb), (d) $CaMoO_4:Er^{3+}/Yb^{3+}$# (CMO:Er/Yb#) and (e) $CaMoO_4:Er^{3+}/Yb^{3+}$# (CMO:Er/Yb##) particles on the samples excited by the 514.5 nm line of an Ar-ion laser at 0.5 mW. The internal modes for the (a) $CaMoO_4$(CMO) particles were detected as $\nu_1(A_g)$, $\nu_3(B_g)$, $\nu_3(E_g)$, $\nu_4(E_g)$, $\nu_4(B_g)$ and $\nu_2(B_g)$ vibrations at 878, 847, 793, 380, 357 and 321 cm^{-1}, respectively. A free rotation mode was detected at 180 cm^{-1} and the external modes were localized at 140 and 109 cm^{-1}. The well-resolved sharp peaks of the $CaMoO_4$ particles indicate the high crystallization of the synthesized particles. The internal vibration mode frequencies are dependent on the lattice parameters and the degree of the partially covalent bond between the cation and molecular ionic group $[MoO_4]^{2-}$. The Raman spectra of the (b) $CaMoO_4:Er^{3+}$ (CMO:Er), (c) $CaMoO_4:Er^{3+}/Yb^{3+}$ (CMO:Er/Yb), (d) $CaMoO_4:Er^{3+}/Yb^{3+}$# (CMO:Er/Yb#) and (e) $CaMoO_4:Er^{3+}/Yb^{3+}$## (CMO:Er/Yb##) particles indicate additional strong peaks at both higher frequencies (618, 575, 492, 420 and 373 cm^{-1}) and lower frequencies (290 and 234 cm^{-1}). The Raman spectra of $CaMoO_4:Er^{3+}$, $CaMoO_4:Er^{3+}/Yb^{3+}$, $CaMoO_4:Er^{3+}/Yb^{3+}$# and $CaMoO_4:Er^{3+}/Yb^{3+}$## particles proved that the doping ions can influence the structure of the host materials. This finding was attributed to the bulk vibration modes as a trace byproduct in the samples.

Conclusions

The UC photoluminescence of Er^{3+}/Yb^{3+} co-doped $CaMoO_4$ ($CaMoO_4:Er^{3+}/Yb^{3+}$) particles was successfully achieved by a cyclic MAM route. Well-crystallized $CaMoO_4:Er^{3+}/Yb^{3+}$# particles were formed after heat-treatment at 600 ºC for 3 h, showing a fine and homogeneous morphology with particle sizes of 1-3 ìm. With excitation at 980 nm, $CaMoO_4:Er^{3+}/Yb^{3+}$# particles exhibited a strong 525-nm emission band and a weak 550-nm emission band in the green region, which were assigned to the $^2H_{11/2} \rightarrow {}^4I_{15/2}$ and $^4S_{3/2} \rightarrow {}^4I_{15/2}$ transitions of Er^{3+} ions, respectively, while a

weak 655-nm emission band in the red region was assigned to the $^4F_{9/2} \rightarrow {}^4I_{15/2}$ transition. The UC intensity of $CaMoO_4:Er^{3+}/Yb^{3+}$# particles was much higher than those of the $CaMoO_4:Er^{3+}$ and $CaMoO_4:Er^{3+}/Yb^{3+}$ particles. The Raman spectra of $CaMoO_4:Er^{3+}$, $CaMoO_4$: Er^{3+}/Yb^{3+}, $CaMoO_4$: Er^{3+}/Yb^{3+}# and $CaMoO_4:Er^{3+}/Yb^{3+}$## particles indicated the detection of additional strong peaks at higher frequencies (618, 575, 492, 420 and 373 cm^{-1}) and at lower frequencies (290 and 234 cm^{-1}). The Raman spectra of $CaMoO_4:Er^{3+}$, $CaMoO_4:Er^{3+}$/ Yb^{3+}, $CaMoO_4$: Er^{3+}/Yb^{3+}# and $CaMoO_4:Er^{3+}/Yb^{3+}$## particles proved that the doping ions can influence the structure of the host materials. This finding was attributed to the bulk vibration modes as a trace byproduct in the samples.

Acknowledgement

This study was supported by Research Program through the Campus Research Foundation funded by Hanseo University in 2012 (121Gonghang03).

References

1. M. Wang, G. Abbineni, A. Clevenger, C. Mao, S. Xu, Nanomedicine: Nanotech. Biology, and Medicine 7 (2011) 710-729.
2. A. Shalav, B.S. Richards, M.A. Green, Solar Ener. Mat. & Solar Cells 91 (2007) 829-842.
3. P. Yu, J. Bi, D.Q. Xiao, L.P. Chen, X.L. Jin, Z.N. Yang, J. Electroceram. 16 (2006) 473-476.
4. J.C. Sczancoski, L.S. Cavalcante, M.R. Joya, J.A. Varela, P.S. Pizani, E. Longo, Chem. Eng. J. 140 (2008) 632-637.
5. T. Thongtem, S. Kungwankunakorn, B. Kuntalue, A. Phuruangrat, S. Thongtem, J. Alloys & Comp. 506 (2010) 475-481.
6. J.H. Ryu, J.W. Yoon, C.S. Lim, W.C. Oh, K.B. Shim, J. Alloys & Comp. 390 (2005) 245-249.
7. J. Sun, J. Xian, H. Du, J. Phys. Chem. of Solids 72 (2011) 207-213.
8. J. Sun, J. Xian, Z. Xia, H. Du, J. Rare Earths 28 (2010) 219-221.
9. V.K. Komarala, Y. Wang, M. Xiao, Chem. Phys. Lett. 490 (2010) 189-193.
10. X. Lin, X. Qiao, X. Fan, Solid State Science 13 (2011) 579-583.
11. L.Y. Zhou, J.S. Wei, F.Z. Gong, J.L. Huang, L.H. Yi, J. Solid State Chem. 181 (2008) 1337-1341.
12. J. Liu, H. Lian, C. Shi, Optical Mat. 29 (2007) 1591-1595.
13. X. Li, Z. Yang, L. Guan, J. Guo, Y. Wang, Q. Guo, J. Alloys & Comp. 478 (2009) 684-686.
14. D. Gao, Y. Li, X. Lai, Y. Wei, J. Bi, Y. Li, M. Liu, Mat. Chem. Phys. 126 (2011) 391-397.
15. Y. Yang, X. Li, W. Feng, W. Yang, W. Li, C. Tao, J. Alloys & Comp. 509 (2011) 845-848.
16. F.B. Cao, L.S. Li, Y.W. Tian, Y.J. Chen, X.R. Wu, Thin Solid Films, 519 (2011) 7971-7976.
17. Y. Jin, J. Zhang, Z. Hao, X. Zhang, X.J. Wang, J. Alloys & Comp. 509 (2011) L348-L351.
18. F. Yu, J. Zuo, Z. Zhao, C. Jiang, Q. Yang, Mat. Res. Bull. 46 (2011) 1327-1332.
19. F. Lei, B. Yan, J. Sol. Sta. Chem. 181 (2008) 855-862.
20. Z.J. Zhang, H.H. Chen, X.X. Yang, J.T. Zhao, Mat. Sci. Eng. B 145 (2007) 34-40.
21. N. Niu, P. Yang, W. Wang, F. He, S. Gai, D. Wang, J. Lin, Mat. Res. Bull. 46 (2011) 333-339.
22. J. Zhang, X. Wang, X. Zhang, X. Zhao, X. Liu, L. Peng, Inorg. Chem. Comm. 14 (2011) 1723-1727.
23. C.S. Lim, Mat. Chem. Phys. 131, (2012) 714-718.
24. S. Das, A.K. Mukhopadhyay, S. Datta, D. Basu, Bull. Mat. Sci. 32 (2009) 1-13.
25. K.P.F. Siqueira, R.L. Moreira, M. Valadares, A. Dias, J. Mat. Sci. 45 (2010) 6083-6093.
26. P. Parhi, T.N. Karthik, V. Manivannan, J. Alloys & Compd. 465 (2008) 380-386.
27. V. Thangadurai, C. Knittlmayer, W. Weppner, Mat. Sci. Eng. B 106 (2004) 228-233.